Preliminary study on ductile fracture of imperfect lattice materials

Xiaodong Cui [a], Zhenyu Xue [a], Yongmao Pei [b], Daining Fang [a,b,∗]

[a] AML, Department of Engineering Mechanics, Tsinghua University, Beijing 100084, China
[b] LTCS, College of Engineering, Peking University, Beijing 100871, China

ABSTRACT

The ductile fracture behavior of two-dimensional imperfect lattice material under dynamic stretching is studied by finite element method using ABAQUS/Explicit code. The simulations are performed with three isotopic lattice materials: the regular hexagonal honeycomb, the Kagome lattice and the regular triangular lattice. All the three lattices are made of an elastic/visco-plastic metal material. Two typical imperfections: vacancy defect and rigid inclusion are introduced separately. The numerical results reveal novel deformation modes and crack growth patterns in the ductile fracture of lattice material. Various crack growth patterns as defined according to their profiles, "X"-type, "Butterfly"-type, "Petal"-type, are observed in different combinations of imperfection type and lattice topology. Crack propagation could induce severe material softening and deduce the plastic dissipation of the lattices. Subsequently, the effects of the strain rate, relative density, microstructure topology, and defect type on the crack growth pattern, the associated macroscopic material softening and the knock-down of total plastic dissipation are investigated.

© 2011 Elsevier Ltd. All rights reserved.

1. Introduction

Lattice materials have significant potentials in engineering applications due to their preferable mechanical performances and multifunctionality (Deshpande et al., 2001; Evans et al., 1998; Wadley, 2006). The macroscopic effective stiffness, strength and yielding of the lattice materials have been systematically investigated by theoretical, numerical and experimental methods (Gibson and Ashby, 1997; Papka and Kyriakides, 1998; Torquato et al., 1998). The effects of imperfection on mechanical behavior of lattice materials were also studied by numerous researchers (Chen et al., 1999; Grenestedt, 1998; Silva et al., 1995; Symons and Fleck, 2008). Further understanding of the damage tolerance and fracture mechanism of lattice materials is essentially important in their practical application.

The brittle fracture of elastic lattice materials has already been detailedly analyzed in previous researches. The macroscopic fracture toughness of hexagonal honeycomb was investigated for elastic brittle material (Gibson and Ashby, 1997; Huang and Gibson, 1991; Maiti et al., 1984). Recently, Fleck and Qiu (2007) simulated the fracture toughness of isotropic lattices: hexagonal honeycomb, triangular lattice and Kagome lattice by finite element analysis and they also provided corresponding analytical prediction. Square lattice was also examined (Alonso and Fleck, 2007). Lipperman et al. (2007a) calculated the fracture toughness of the above four lattices

by means of the discrete Fourier transform. They also studied the nucleation and propagation of cracks in these cellular materials (Lipperman et al., 2007b). Slepyan (2001a,b,c, 2005) investigated the dynamic crack propagation in elastic lattices analytically. However, the ductile fracture behavior of lattice materials has not been investigated, except for the numerical study of Schmidt and Fleck (2001) on regular and irregular hexagonal honeycomb.

From a microscopic point of view, ductile failure of solid material is usually characterized by three stages: nucleation, growth and coalescence of microscopic voids, which are induced by the existence of inclusions and second phase particles. Because of the high porosity of lattice material, its ductile fracture behavior is quite different from that of the homogeneous metal material. While the ductile fracture of solid metal materials has been well studied, the growth of micro voids induced by structural imperfection and the propagation of induced cracks in lattice materials are still unclear. This is the objective of the present paper. To study the ductile fracture behaviors of imperfect metal lattice materials, the dynamic stretching is simulated by using finite element method. In Section 2, the numerical model is described in detail. The simulated results are discussed in Section 3, including the growth patterns of induced cracks, the associated material softening and the descent of the energy absorption ability. Finally, the conclusions are summarized in Section 4.

2. Finite element simulation

Three isotropic lattice materials with vacancy defect or rigid inclusion are investigated by means of finite element method.

∗ Corresponding author at: AML, Department of Engineering Mechanics, Tsinghua University, Beijing 100084, China. Tel./fax: +86 10 62772923.
 E-mail address: fangdn@pku.edu.cn (D. Fang).

The vacancy defect/rigid inclusion are introduced by removing/rigidifying one joint and the connected cell walls, which are represented by dashed lines in Fig. 1. It should be noticed that, to maintain the structural symmetry, two joints and the connected cell walls are removed from hexagonal honeycomb.

The finite element model of lattices is composed of 50 cells by 50 cells. The walls in perfect cells have a length of l and a width of t. The imperfection is created by varying the width of cell walls. The walls with a width much smaller than t denote vacancy defects, while the walls with a width much larger than t denote rigid inclusions.

The hexagonal honeycomb under dynamic stretching along x_2-axis is taken as an example, and its undeformed shape is sketched in Fig. 2. The displacement in x_1-direction of the joints at the two vertical surfaces is restricted to avoid the inertial effect and boundary layer effect. If the two vertical surfaces were set free, the inertial pressure would have been induced by Poisson's effect, and uniform macroscopic deformation could not be achieved. Boundary layer would also emerge at the free boundaries under external loading (Fleck and Qiu, 2007). Based on the fundamental solution of imperfection-free plate under uniform stretching, proposed by Shenoy and Freund (1999), an initial velocity field is imposed to ensure uniform deformation field, i.e.

$$V(x_2) = \dot{\bar{\varepsilon}}_0 x_2, \tag{1}$$

where $\dot{\bar{\varepsilon}}_0 = V_0/2L_2$, is the nominal strain rate of lattice material, L_2 is the width of the lattice, and $V_0/2$ is the magnitude of velocity at the stretching ends.

The constitutive relation of the solid material is characterized by Johnson–Cook model (JC model), which involves linear thermo-elasticity, yielding plastic flow, isotropic strain hardening, strain rate effect, and softening due to adiabatic heating and damage. In the JC model, the equivalent von Mises flow stress is given by

$$\sigma_Y = [A + B(\bar{\varepsilon}^{pl})^n]\left[1 + C\ln\left(\frac{\dot{\bar{\varepsilon}}^{pl}}{\dot{\varepsilon}_0}\right)\right][1 - (T_H)^m], \tag{2}$$

where A, B, C, n, and m are material parameters, $\bar{\varepsilon}^{pl}$ is the equivalent plastic strain, $\dot{\bar{\varepsilon}}^{pl}$ is equivalent plastic strain rate, $\dot{\varepsilon}_0$ is a reference strain rate, and T_H is the non-dimensional temperature defined as follows,

$$T_H = \frac{T - T_R}{T_M - T_R}, \tag{3}$$

where T is the current temperature, T_M is the melting point temperature, and T_R is the reference temperature.

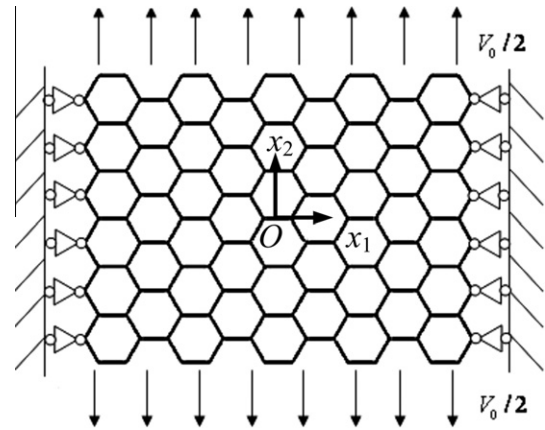To simulate the failure of metal material, a fracture model proposed by Johnson and Cook based on cumulative damage is

Fig. 2. Schematic diagram of hexagonal honeycomb under dynamic stretching along x_2-axis.

adopted (Johnson and Cook, 1985). Failure occurs when a damage parameter D exceeds the critical value 1. The damage parameter D, is defined as follows,

$$D = \sum\left(\frac{\Delta\bar{\varepsilon}^{pl}}{\bar{\varepsilon}_f^{pl}}\right), \tag{4}$$

where $\Delta\bar{\varepsilon}^{pl}$ is an increment of the equivalent plastic strain, $\bar{\varepsilon}_f^{pl}$ is the equivalent strain at failure, and $\bar{\varepsilon}_f^{pl}$ is assumed to be dependent on a non-dimensional plastic strain rate. When the temperature effect is not considered, the equivalent failure strain is given by

$$\bar{\varepsilon}_f^{pl}\left[d_1 + d_2\exp\left(d_3\frac{P}{\sigma_Y}\right)\right]\left[1 + d_4\ln\left(\frac{\dot{\bar{\varepsilon}}^{pl}}{\dot{\varepsilon}_0}\right)\right], \tag{5}$$

where d_1, d_2, d_3 and d_4 are material constants, and P is the mean stress. When the failure criterion is met, the "element kill" algorithm available in ABAQUS can be used to delete the failure elements from the mesh. It ensures that the mean stress in killed elements is zero during subsequent analysis (ABAQUS, 2004). The material investigated in the present study is 2024-T351 aluminum alloy, and its material parameters are given by Johnson and Cook (1983), as listed in Table 1.

The simulation of the above computational problem is performed by means of the commercially available FEM code ABAQUS Explicit (version 6.5). Timoshenko beam elements with linear interpolation functions (element type B21 in ABAQUS) are adopted to ensure the accuracy of the simulations, and numerical convergence is confirmed by refining the meshes.
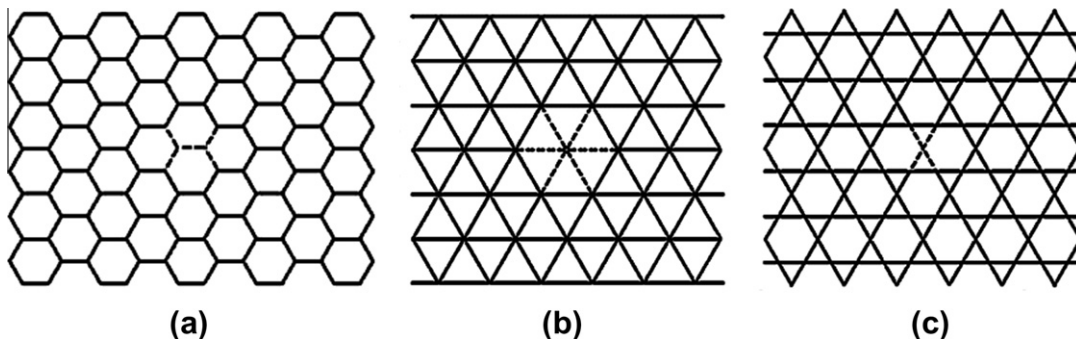

Fig. 1. Three isotropic two dimensional lattice materials with imperfection: (a) hexagonal honeycomb; (b) triangular lattice; (c) Kagome lattice. (The dashed lines denote the imperfect bars.)

Table 1
Johnson–Cook parameters for aluminum used in the numerical analyses.

E (GPa)	v	ρ (kg/m^3)	$\dot{\varepsilon}_0$ (1/s)	C	C_p (J/kg K)
73.08	0.33	2770	1.0	0.015	875
T_M (K)	T_R (K)	m	A (MPa)	B (MPa)	n
775	294	1.0	265	426	0.34
d_1	d_2	d_3	d_4	d_5	χ
0.13	0.13	−1.5	0.011	0.0	0.9

3. Results and discussion

The dynamic stretching are simulated for the three lattices under strain rate $\dot{\bar{\varepsilon}}_0 = 10\,\text{s}^{-1}$, $\dot{\bar{\varepsilon}}_0 = 100\,\text{s}^{-1}$ and $\dot{\bar{\varepsilon}}_0 = 1000\,\text{s}^{-1}$, respectively. Unexpected crack growth patterns are found from the simulations. The propagating cracks result in substantial material softening, and reduce the energy dissipated by the deformation of the lattice materials. The crack growth pattern, the associated material softening and knock-down of energy absorption are discussed separately in the following sections.

3.1. Crack growth pattern

3.1.1. Triangular lattice

The deformation of triangular lattice with vacancy defect under dynamic stretching along x_2-axis is shown in Fig. 3. The relative density of the triangular lattice is $\bar{\rho} = 10\%$, and three nominal strain rates, $\dot{\bar{\varepsilon}}_0 = 10\,\text{s}^{-1}$, $\dot{\bar{\varepsilon}}_0 = 100\,\text{s}^{-1}$ and $\dot{\bar{\varepsilon}}_0 = 1000\,\text{s}^{-1}$ are considered, respectively. It can be seen that a crack growth pattern, named as "X"-type, is induced at low strain rate. The fracture initiates at the inclined cell walls near the defect, and four induced cracks develop along the $\pm\pi/3$ axis and $\pm2\pi/3$ axis, respectively. The final crack length at the global failure of the lattice decreases with the increasing of strain rate. When the strain rate reaches to enough high value, no apparent crack is formed before the global fracture of the lattice. It is because that the maximum crack propagation speed is the Rayleigh wave speed, which is predicted by continuum mechanics (Freund, 1990). The propagation time of crack decreases with the increasing of strain rate. When the strain rate is high enough, there is no enough time left for the crack to propagate before the global fracture of the lattice. This general conclusion is also valid for the hexagonal honeycomb and the Kagome lattice. Therefore, the dynamic stretching under nominal strain rate $\dot{\bar{\varepsilon}}_0 = 10\,\text{s}^{-1}$, is adopted in the following simulations.

The simulation of triangular lattice with a different relative density of $\bar{\rho} = 2\%$ is also performed. The similarity of the deformation mode with that in the case of relative density $\bar{\rho} = 10\%$ indicates the independence of crack growth pattern on relative density for the triangular lattice.

For rigid inclusion, it can be seen from Fig. 4 that the initial fracture occurs at the inclined walls next to the inclusion in the vertical direction, and the induced cracks grow as an "X"-type as well. It should be noticed that the nominal strain at the initial fracture of the lattice with rigid inclusion is much larger than that of the lattice with vacancy defect.
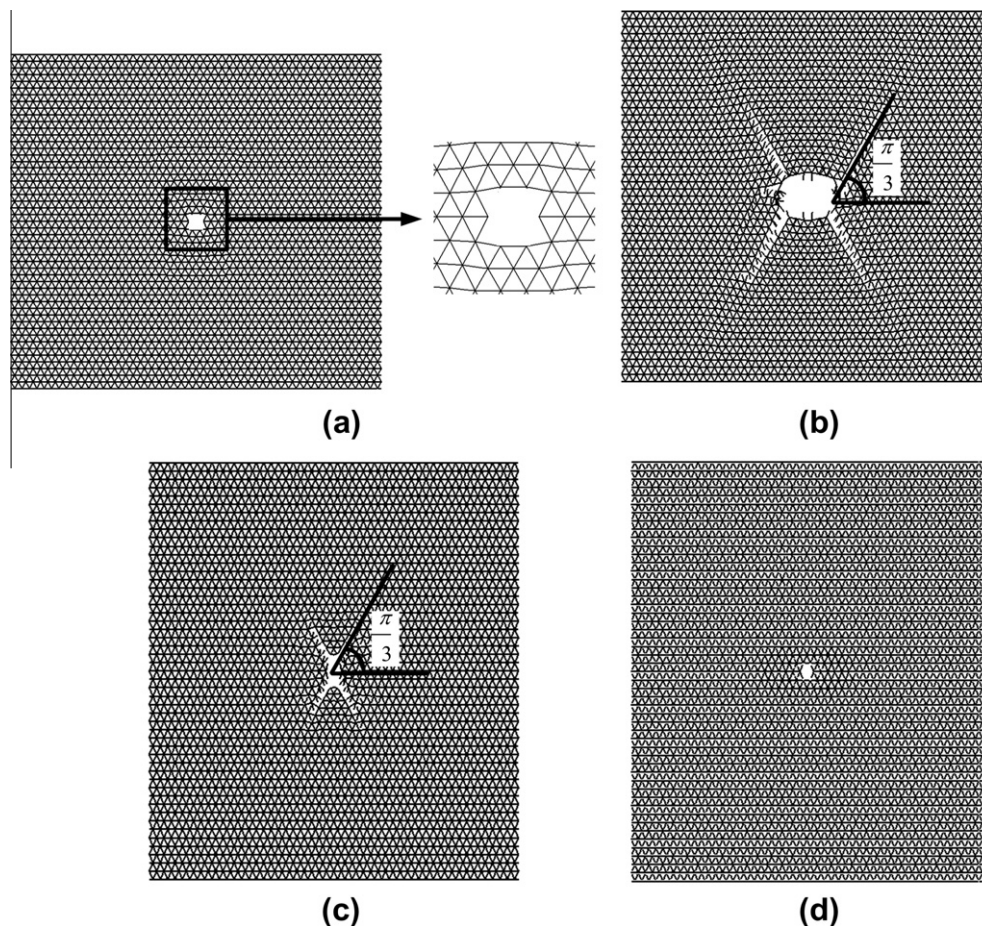

Fig. 3. Dynamic stretching of triangular lattice with vacancy defect along x_2-axis: (a) the initial fracture of cell wall; (b) "X"-type crack under $\dot{\bar{\varepsilon}}_0 = 10\,\text{s}^{-1}$; (c) "X"-type crack under $\dot{\bar{\varepsilon}}_0 = 100\,\text{s}^{-1}$; (d) global failure under $\dot{\bar{\varepsilon}}_0 = 1000\,\text{s}^{-1}$. The relative density is $\bar{\rho} = 10\%$.
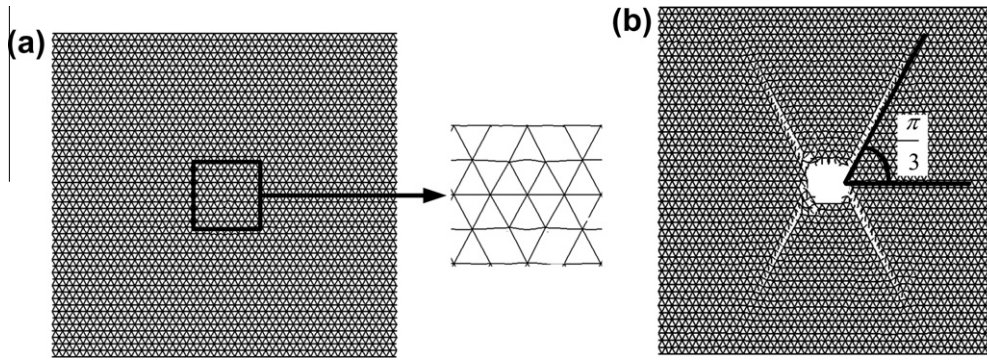
Fig. 4. Dynamic stretching of triangular lattice with rigid inclusion along x_2-axis: (a) the initial fracture of cell wall; (b) "X"-type crack. The relative density is $\overline{\rho} = 10\%$, and the nominal strain rate is $\dot{\overline{\varepsilon}}_0 = 10 \, \text{s}^{-1}$.

3.1.2. Hexagonal honeycomb

Compared with the triangular lattice, the hexagonal honeycomb exhibits a significantly different behavior. The result from vacancy defect is shown in Fig. 5. It can be seen that the fracture occurs at the inclined cell walls near the defect in the horizontal direction, and a "Butterfly"-type crack growth pattern develops under the stretching along x_2-axis. The crack growth directions are along the $\pm\pi/6$ axis and $\pm5\pi/6$ axis, respectively. The finite element simulations show that the crack growth pattern of the hexagonal honeycomb is also independent on its relative density. For rigid inclusion, with the failure initiating at the inclined cell walls next to the defect in the vertical direction, a "Petal"-type crack formed, which is sketched in Fig. 6.

The hexagonal honeycomb exhibit a crack growth pattern with opening trend because of its bending dominated deformation mechanism. The constraint of the cell walls near the crack is released as the crack grows, and the deformation becomes much easier. Therefore, the distance between the two sides of the crack increases as the crack grows.

3.1.3. Kagome lattice

Different from the triangular lattice and the hexagonal honeycomb, the Kagome lattice exhibits a relative density dependent behavior under dynamic stretching.

For vacancy defect, the fracture occurs at the inclined cell walls near the defect in the horizontal direction. At a relative density of $\overline{\rho} = 10\%$, a central horizontal crack is generated from the defect in the Kagome lattice at first, and then four cracks develop along the $\pm \pi/3$ axis and $\pm2\pi/3$ axis (see Fig. 7). The cracks form an "X"-Type crack pattern. When the relative density is reduced to $\overline{\rho} = 2\%$, no obvious horizontal crack develops (see Fig. 8a). As the relative density is reduced to $\overline{\rho} = 1\%$, a crack growth pattern between the "Butterfly"-type and "X"-type is generated (see Fig. 8b). In the Kagome lattice, the mechanical behavior of the region near the vacancy defect is dominated by the combination of bending and stretching. When the relative density is small, bending effect becomes dominant, and the crack growth pattern is similar to that of the hexagonal honeycomb. With the increase of the relative density, the stretching gradually plays a dominant role and the crack growth pattern turns to be the same as the triangular lattice. For convenience, only the Kagome lattice with the relative density $\overline{\rho} = 10\%$ is discussed in the following sections.

The deformation of Kagome lattice with rigid inclusion is shown in Fig. 9. It can be seen that the failure initiates at the inclined cell walls next to the defect in the vertical direction. Subsequently, an "X"-type crack forms in a rapid way.

3.1.4. Compared with the brittle lattices

In the study of Lipperman et al. (2007b), the directions of crack propagation also depend upon the lattice microstructure.

In the triangular and Kagome lattice, the crack was aligned perpendicularly to the loading for uniaxial loading. In hexagonal honeycombs the crack was inclined by 30° to the load direction. The common phenomenon is a macrocrack propagating in the weakest direction. However, mirror symmetrical cracks are developed for the three lattices in our study. This difference is mainly due to the different nature of the parent materials. The brittle material is considered as complete failure when the largest normal tensile reaches the critical failure stress, thus the cracks propagate by sequential failure of critical elements. But the failure of metal materials is based on cumulative damage. The ductile elements have substantial load bearing ability after yielding. The developing crack won't stop the damage accumulating in other elements, so other cracks can be developed when the failure condition is met.

3.2. Material softening

As mentioned in Section 3.1, the lattice materials display various crack growth patterns, which are quite different from the homogeneous ductile materials. The developed cracks will induce significant material softening in the lattice materials.

For perfect lattice material, the macroscopic stress can be derived by analyzing a representative unit cell due to its periodicity. Take the triangular lattice as example. The deformation of a unit cell of triangular lattice under stretching is shown in Fig. 10. Zhang et al. proposed the ultimate yielding of statically indeterminate lattice, implying its loading bearing capability after initial yielding (Zhang et al., 2008). The initial and ultimate yielding must be considered for the triangular lattice.

Under quasi-static stretching along x_2-axis, the initial and ultimate yielding occur simultaneously. The yielding stress of the unit cell can be written as

$$\left(\sigma_y^t\right)_2 = \frac{\sqrt{3}t}{l}\sigma_{ys} = 0.5\overline{\rho}\sigma_{ys}, \tag{6}$$

where σ_{ys} is the yielding strength of the solid material. Under quasi-static stretching along x_1-axis, the initial yielding of the unit cell occurs when the horizontal struts yield, and the ultimate yielding is achieved when the inclined struts yield either. Thus, the initial and ultimate yielding stress of the unit cell can be respectively expressed as

$$\left(\sigma_y^t\right)_2 = \frac{5\sqrt{3}t}{6l}\sigma_{ys} = \frac{5}{12}\overline{\rho}\sigma_{ys} \tag{7}$$

and

$$\left(\sigma_y^t\right)_2 = \frac{\sqrt{3}t}{l}\sigma_{ys} = 0.5\overline{\rho}\sigma_{ys}. \tag{8}$$
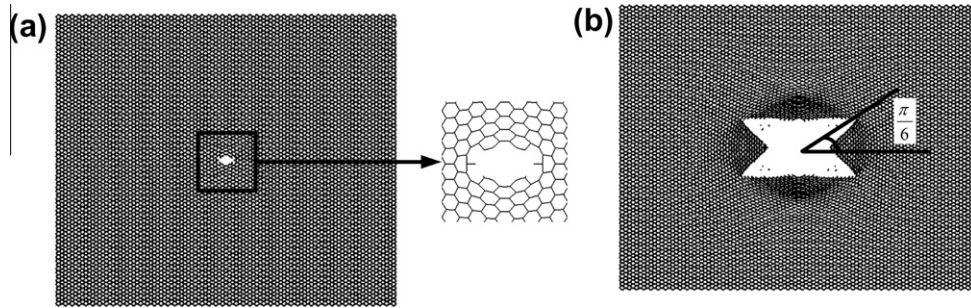
Fig. 5. Dynamic stretching of hexagonal honeycomb with vacancy defect along x_2-axis: (a) the initial fracture of cell wall; (b) "Butterfly"-type crack. The relative density is $\overline{\rho} = 10\%$, and the nominal strain rate is $\dot{\overline{\varepsilon}}_0 = 10 \text{ s}^{-1}$.
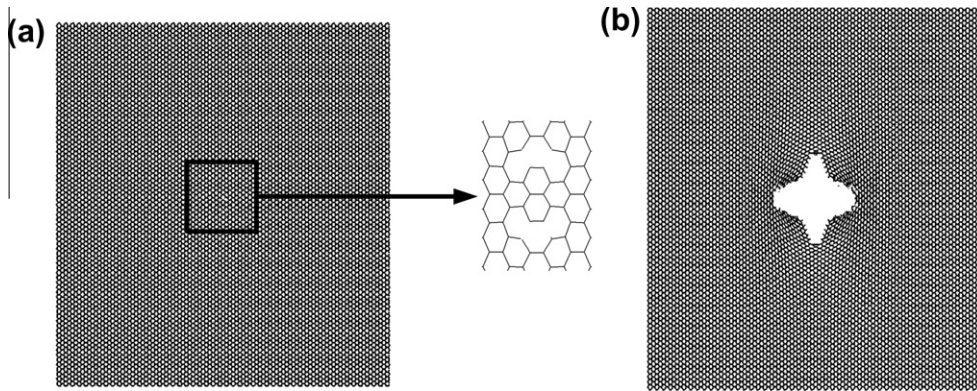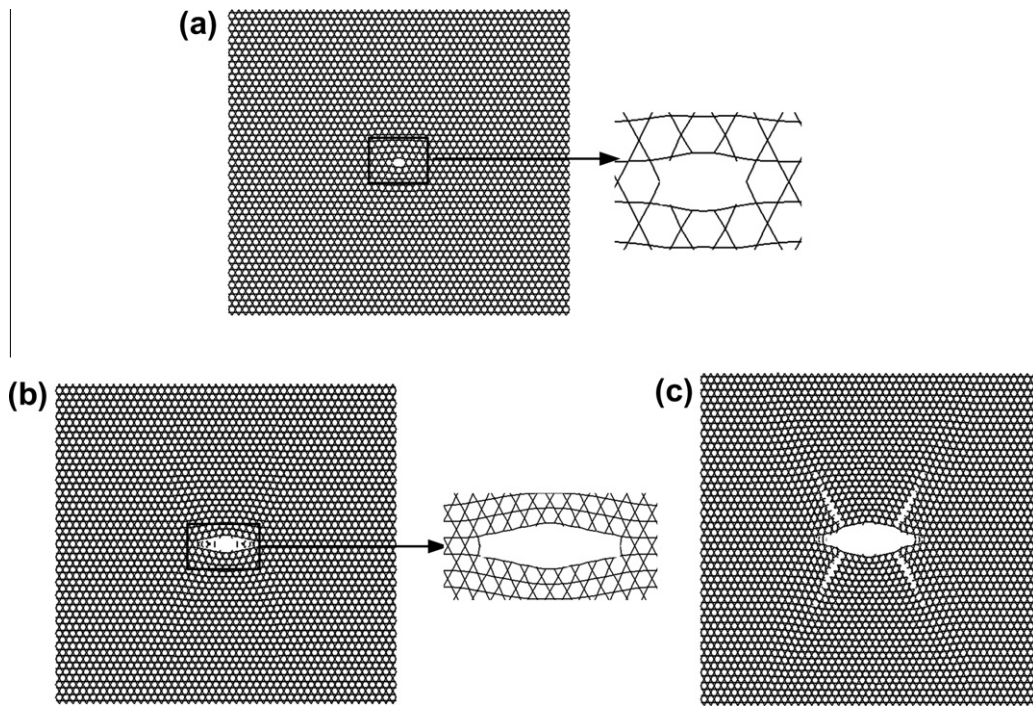

Fig. 6. Dynamic stretching of hexagonal honeycomb with rigid inclusion along x_2-axis: (a) the initial fracture of cell wall; (b) "Petal"-type crack. The relative density is $\overline{\rho} = 10\%$, and the nominal strain rate is $\dot{\overline{\varepsilon}}_0 = 10 \text{ s}^{-1}$.

Fig. 7. Dynamic stretching of Kagome lattice with vacancy defect along x_2-axis: (a) the initial fracture of cell wall; (b) a horizontal crack; (c) "X"-type crack. The relative density is $\overline{\rho} = 10\%$, and the nominal strain rate is $\dot{\overline{\varepsilon}}_0 = 10 \text{ s}^{-1}$.

It can be concluded that both the ultimate yielding stress of the triangular lattice under quasi-static stretching along x_1-axis and x_2-axis are $0.5\overline{\rho}\sigma_{ys}$. With the same analyzing method as the triangular lattice, the yielding stresses of the hexagonal honeycomb and Kagome lattice can be derived, and they turn out to be of the same value as that of the triangular lattice. Therefore, the nominal far field stress σ_∞ of the imperfect lattices is normalized by $\overline{\sigma}_\infty = \sigma_\infty/(0.5\overline{\rho}\sigma_{ys})$.
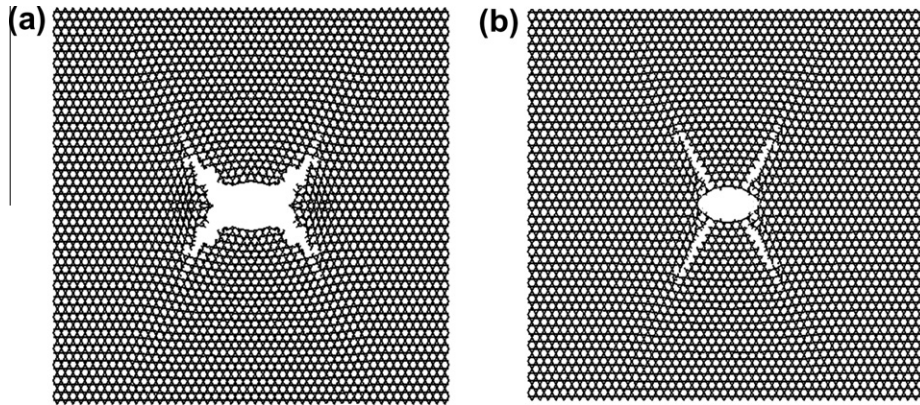
Fig. 8. Dynamic stretching of Kagome lattice with vacancy defect along x_2-axis: (a) the relative density is $\overline{\rho} = 1\%$; (b) the relative density is $\overline{\rho} = 2\%$. The nominal strain rate is $\dot{\overline{\varepsilon}}_0 = 10\ \text{s}^{-1}$.
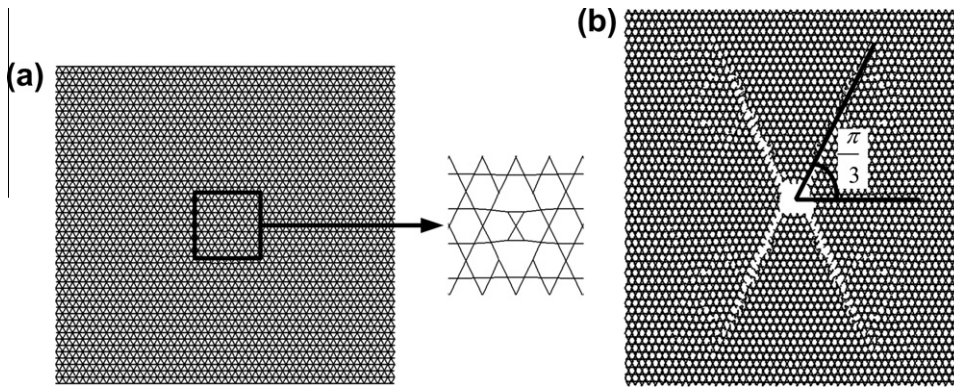

Fig. 9. Dynamic stretching of Kagome lattice with rigid inclusion along x_2-axis: (a) the initial fracture of cell wall; (b) "X"-type crack. The relative density is $\overline{\rho} = 10\%$, and the nominal strain rate is $\dot{\overline{\varepsilon}}_0 = 10\ \text{s}^{-1}$.
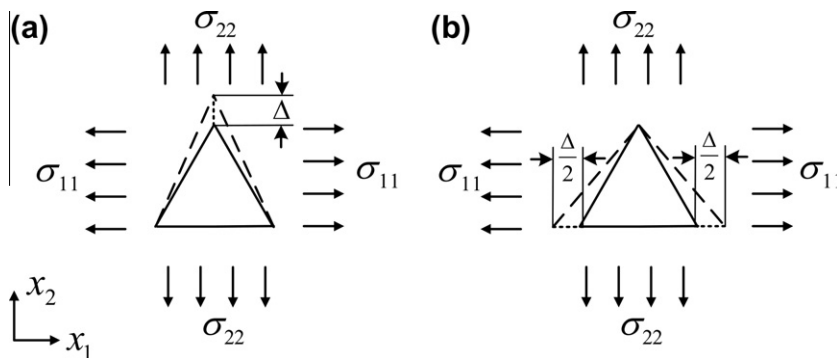

Fig. 10. Unit cell of the triangular lattice under stretching: (a) along x_2-axis; (b) along x_1-axis.

As mentioned in Section 2, the inertia effects are neglected in the finite element simulations. Considering the constitutive relation of the parent material (Eq. (2)), under dynamic stretching, the ultimate yielding stress can be estimated by

$$\left(\sigma_y^*\right)^u \cong 0.5\overline{\rho}^* \sigma_{ys}\left[1 + C\ln\left(\frac{\dot{\overline{\varepsilon}}_0}{\dot{\varepsilon}_0}\right)\right], \tag{9}$$

where the superscript "∗" denotes the type of lattice materials. The comparison of the prediction with finite element simulation is plotted in Fig. 11. The good agreement implies that the estimation indeed provides a good prediction of the yielding stress.

The normalized average stress versus nominal strain curves of the triangular lattice with vacancy defect under dynamic stretching along x_2-axis are shown in Fig. 11, where the relative density is $\overline{\rho} = 10\%$. The curve of the corresponding perfect triangular lattice is also shown in the figure to demonstrate the material softening behavior. It can be seen that at a lower strain rate of $\dot{\overline{\varepsilon}}_0 = 10\ \text{s}^{-1}$, a rapid drop in average stress occurs when the nominal strain reaches about 0.13, which is far less than the failure strain. But at much higher strain rate, such as $\dot{\overline{\varepsilon}}_0 = 100\text{s}^{-1}$ and $\dot{\overline{\varepsilon}}_0 = 1000\ \text{s}^{-1}$, no obvious material softening is observed.

The Kagome lattice with vacancy defect exhibits similar material softening behavior, even when it has different relative densities. The results are shown in Fig. 12. The softening initiates are
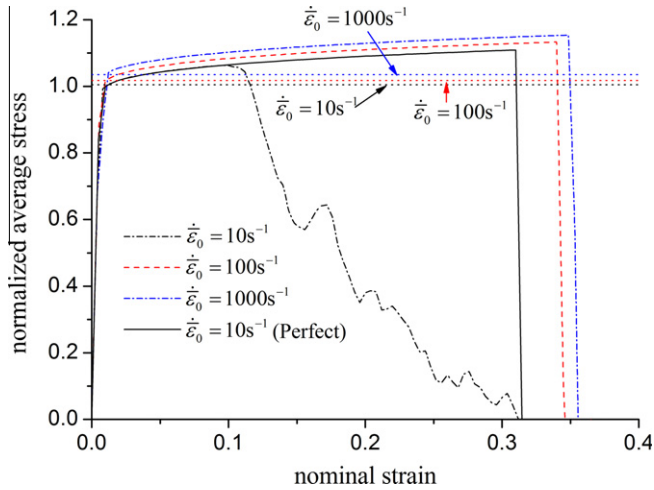
Fig. 11. The normalized average stress vs. nominal strain for the triangular lattice with vacancy defect under dynamic stretching along x_2-axis. The relative density is $\bar{\rho} = 10\%$. The dashed lines are the predictions of the normalized yielding stress from Eq. (9).

Fig. 12. The normalized average stress vs. nominal strain for the Kagome lattice with vacancy defect under dynamic stretching along x_2-axis. The nominal strain rate is $\dot{\bar{\varepsilon}}_0 = 10\,\mathrm{s}^{-1}$.

at about the same nominal strain, but due to the varied crack growth patterns, apparent difference occurs in the subsequent softening process. The material softening in the Kagome lattice with $\bar{\rho} = 10\%$ develops at a higher speed. It is because that the crack tip influencing zone is much larger when the relative density of the Kagome lattice is smaller, and the larger zone can dissipate more energy in the crack growth procedure.

The curves of normalized average stress versus the nominal strain for the three lattice materials with or without imperfection are shown in Fig. 13. It can be concluded that:

(1) For vacancy defect, material softening starts approximately at the same nominal strain. The average stress in the hexagonal honeycomb decreases more quickly, while that of the other two lattices decreases approximately in the same manner.

(2) For rigid inclusion, material softening initiates at a larger nominal strain. The nominal strain corresponding to the appearance of softening for the triangular lattice is the smallest, and the hexagonal honeycomb has no obvious material softening.

3.3. Plastic dissipation

Plastic dissipation is the most significant energy absorbing mechanism of metal lattice materials. However, material softening can induce a substantial knock-down in the plastic dissipation of lattice materials and reduce their energy absorbing ability. In this section, the plastic dissipation of imperfect lattices is evaluated by normalization of $\overline{E_p} = E_p/E_p^{perfect}$, where $E_p^{perfect}$ denotes the ultimate plastic dissipation of the corresponding perfect lattice, when it reaches global fracture under the same condition. The simulation results from the dynamic stretching of the three perfect lattices with the same relative density imply that their ultimate plastic dissipations have almost equivalent value. Therefore, the plastic dissipation of the three imperfect lattices can be evaluated under the same standard.

The normalized plastic dissipation versus nominal strain curves of the triangular lattice with vacancy defect under dynamic stretching with different strain rates are shown in Fig. 14. It can be seen that the imperfect lattice has an approximate 30% knock-down in ultimate plastic dissipation at a strain rate of
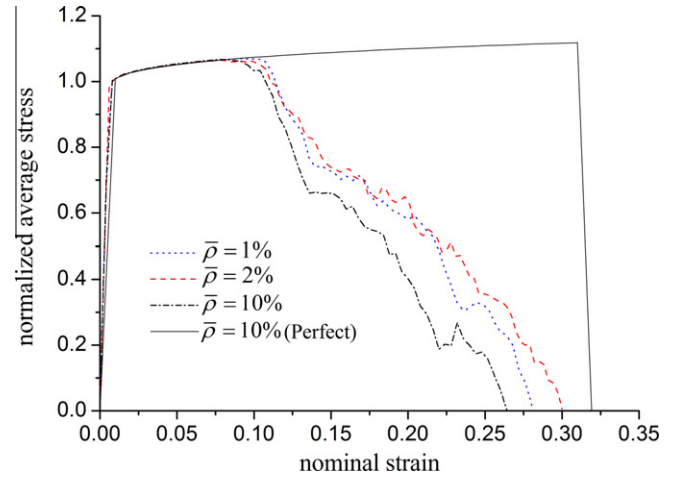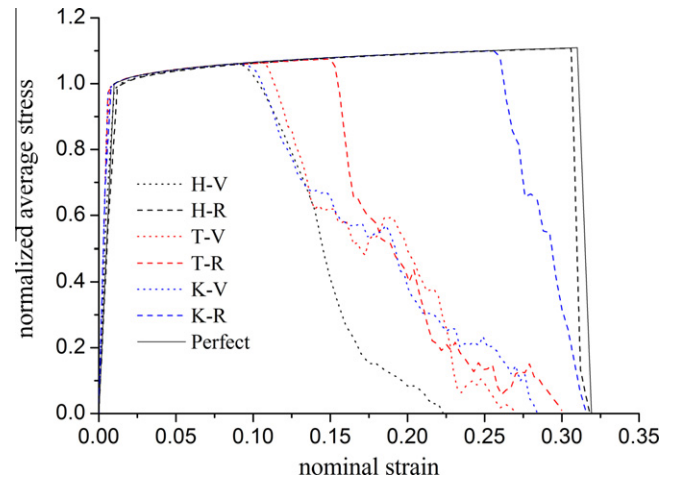

Fig. 13. The normalized average stress vs. nominal strain for the lattices under dynamic stretching along x_2-axis. The relative density is $\bar{\rho} = 10\%$ and the nominal strain rate is $\dot{\bar{\varepsilon}}_0 = 10\,\mathrm{s}^{-1}$. (For convenience, Hexagonal honeycomb, triangular lattice and Kagome lattice are represented by H, T and K, respectively. Vacancy defect and rigid inclusion are represented by V and R, respectively).
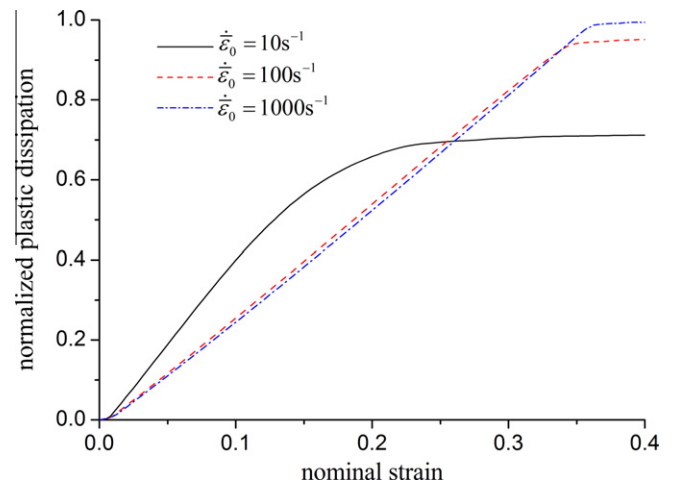

Fig. 14. The normalized plastic dissipation vs. nominal strain for the triangular lattice with vacancy defect under dynamic stretching along x_2-axis. The relative density is $\bar{\rho} = 10\%$.

$\dot{\bar{\varepsilon}}_0 = 10 \text{ s}^{-1}$, while there is no obvious decrease at much higher strain rate, such as $\dot{\bar{\varepsilon}}_0 = 100 \text{ s}^{-1}$ and $\dot{\bar{\varepsilon}}_0 = 1000 \text{ s}^{-1}$. It implies that small defect almost has no effect on the energy absorption of the lattice materials under high strain rate.

The relative density has less effect on the plastic dissipation of the Kagome lattice with vacancy defect, compared with its effect on the crack growth pattern. Both the defect affected region and the bending effect depend on the relative density for the imperfect Kagome lattice. They are competitive mechanisms to decide the plastic dissipation of the Kagome lattice. As shown in Fig. 15, neither the Kagome with relative density $\bar{\rho} = 10\%$ nor the one with $\bar{\rho} = 1\%$ possesses the largest ultimate plastic dissipation. In common, all the three Kagome lattices have an approximate 50% knock-down in ultimate plastic dissipation.

The plastic dissipation curves of the three types of lattice materials are sketched in Fig. 16 to investigate the topology and defect type effects. It can be concluded that:

(1) The ultimate plastic dissipation of the lattice material with rigid inclusion is larger than that of the one with vacancy defect. It implies that the lattice material with rigid inclusion has greater energy absorption ability.

Fig. 15. The normalized plastic dissipation vs. nominal strain for the Kagome lattice with vacancy defect under dynamic stretching along x_2-axis. The nominal strain rate is $\dot{\bar{\varepsilon}}_0 = 10 \text{ s}^{-1}$.

Fig. 16. The normalized plastic dissipation vs. nominal strain for the imperfect lattices under dynamic stretching along x_2-axis. The relative density is $\bar{\rho} = 10\%$, and the nominal strain rate is $\dot{\bar{\varepsilon}}_0 = 10 \text{ s}^{-1}$.

(2) As mentioned in Section 3.2, material softening starts approximately at the same nominal strain for the three lattices with vacancy defect. The deformation mechanism of crack growth determines the ultimate plastic dissipation. The stretching dominant deformation grants the triangular lattice the largest ultimate plastic dissipation. The bending dominant behavior gives the hexagonal honeycomb the weakest energy absorption ability. The combined stretching and bending dominated behavior puts the Kagome lattice in a middle position.

(3) For the rigid inclusion, the nominal strain corresponding to the initial of material softening is the decisive factor. The triangular lattice starts softening at the smallest nominal strain, and it has the weakest energy absorption ability. On the contrary, the hexagonal honeycomb has the greatest energy absorption ability due to the largest nominal strain.

4. Conclusions

The ductile fracture of two-dimensional lattice materials exhibits a widely different behavior under dynamic stretching, compared with brittle lattices and homogeneous solid material. Typical crack growth patterns, such as "X"-type, "Butterfly"-type, and "Petal"-type are observed by FEM simulations. The distinctive types of cracks induce substantial material softening and knock-down in the plastic dissipation of lattice materials. Further discussions are about the effects of strain rate, relative density, microstructure topology, and defect type on the deformation behavior of lattices.

The strain rate has no apparent effect on the crack growth pattern when it is low. But at a higher strain rate, there is no abundant time for crack propagation before the ultimate fracture of the lattices. Hence, the imperfection can hardly induce obvious material softening, thus it has little effect on the plastic dissipation of the lattices.

The relative density plays a substantial role in the fracture behavior of the Kagome lattice due to its combination of stretching and bending dominant deformation mechanism, but it has almost no effect on the triangular lattice or hexagonal honeycomb.

The deformation mechanism of the lattice materials, which is the crucial factor to determine their fracture behavior, mainly depends on the combination of microstructure topology and the defect type. The crack initiates at a larger strain in the lattice with rigid inclusion than that of the one with vacancy defect. Accordingly, the material softening occurs later and the ultimate plastic dissipation is larger.

For vacancy defect, the crack and the induced material softening starts approximately at the same nominal strain in the lattices. The deformation mechanism of crack growth determines the ultimate plastic dissipation. The stretching dominant behavior induces a tight "X"-type crack, and grants the triangular lattice the largest ultimate plastic dissipation. The bending dominant behavior induces a wide open "Butterfly"-type crack, and gives the hexagonal honeycomb the weakest energy absorption ability. The combined stretching and bending dominated behavior induces an intermediate crack growth pattern between the above two, and puts the Kagome lattice in a middle position.

For the rigid inclusion, the nominal strain corresponding to the initial of crack and material softening is the decisive factor. The triangular lattice starts softening at the smallest nominal strain with an "X"-type crack, and has the weakest energy absorption ability. On the contrary, the hexagonal honeycomb has the greatest energy absorption ability due to the largest softening initial strain with a "Petal"-type crack.
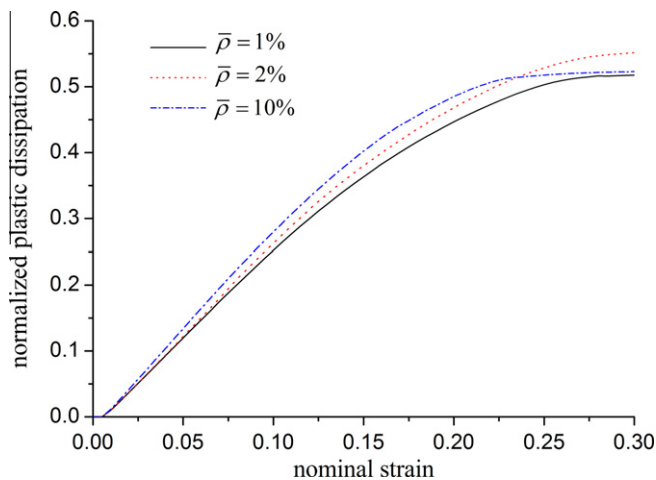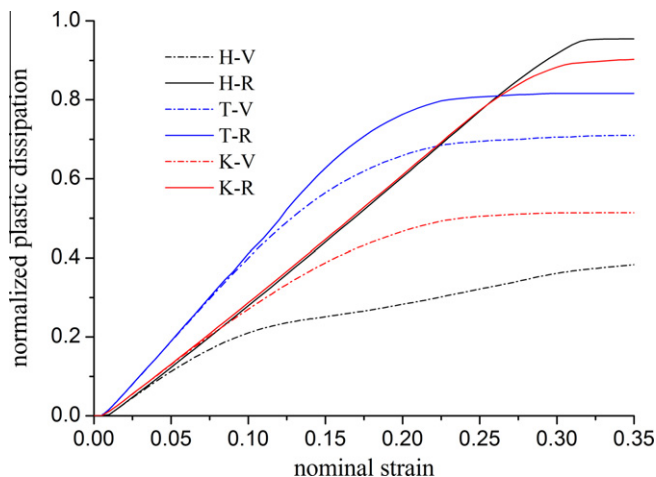
Acknowledgements

References

ABAQUS, 2004. ABAQUS/Explicit User's Manual Version 6.5. ABAQUS Inc.

Alonso, I.Q., Fleck, N.A., 2007. Damage tolerance of an elastic-brittle diamond-celled honeycomb. Scr. Mater. 56, 693–696.

Chen, C., Lu, T.J., Fleck, N.A., 1999. Effect of imperfections on the yielding of two-dimensional foams. J. Mech. Phys. Solids 47, 2235–2272.

Deshpande, V.S., Fleck, N.A., Ashby, M.F., 2001. Effective properties of the octet-truss lattice material. J. Mech. Phys. Solids 49, 1747–1769.

Evans, A.G., Hutchinson, J.W., Ashby, M.F., 1998. Multifunctionality of cellular metal systems. Prog. Mater. Sci. 43, 171–221.

Fleck, N.A., Qiu, X.M., 2007. The damage tolerance of elastic-brittle, two-dimensional isotropic lattices. J. Mech. Phys. Solids 55, 562–588.

Freund, L.B., 1990. Dynamical Fracture Mechanics. Cambridge University Press, New York.

Gibson, L.J., Ashby, M.F., 1997. Cellular Solids: Structure and Properties. Cambridge University Press, Cambridge.

Grenestedt, J.L., 1998. Influence of imperfections on effective properties of cellular solids. Mater. Res. Soc. Symp. Proc. 521, 3–13.

Huang, J.S., Gibson, L.J., 1991. Fracture-toughness of brittle honeycombs. Acta Metall. Mater. 39, 1617–1626.

Johnson, G.R., Cook, W.H., 1983. A constitutive model and data for metals subject to large strains, high strain rates and high temperatures. In: Seventh International Symposium on Ballistics, The Hague, The Netherlands.

Johnson, G.R., Cook, W.H., 1985. Fracture characteristics of 3 metals subjected to various strains, strain rates, temperatures and pressures. Eng. Fract. Mech. 21, 31–48.

Lipperman, F., Ryvkin, M., Fuchs, M.B., 2007a. Fracture toughness of two-dimensional cellular material with periodic microstructure. Int. J. Fract. 146, 279–290.

Lipperman, F., Ryvkin, M., Fuchs, M.B., 2007b. Nucleation of cracks in two-dimensional periodic cellular materials. Comput. Mech. 39, 127–139.

Maiti, S.K., Ashby, M.F., Gibson, L.J., 1984. Fracture-toughness of brittle cellular solids. Scripta Metall. Mater. 18, 213–217.

Papka, S.D., Kyriakides, S., 1998. Experiments and full-scale numerical simulations of in-plane crushing of a honeycomb. Acta Mater. 46, 2765–2776.

Schmidt, I., Fleck, N.A., 2001. Ductile fracture of two-dimensional cellular structures. Int. J. Fract. 117, 327–342.

Shenoy, V.B., Freund, L.B., 1999. Necking bifurcations during high strain rate extension. J. Mech. Phys. Solids 47, 2209–2233.

Silva, M.J., Hayes, W.C., Gibson, L.J., 1995. The effects of non-periodic microstructure on the elastic properties of 2-dimensional cellular solids. Int. J. Mech. Sci. 37, 1161–1177.

Slepyan, L.I., 2001a. Feeding and dissipative waves in fracture and phase transition. I. Some 1D structures and a square-cell lattice. J. Mech. Phys. Solids 49, 469–511.

Slepyan, L.I., 2001b. Feeding and dissipative waves in fracture and phase transition. II. Phase-transition waves. J. Mech. Phys. Solids 49, 513–550.

Slepyan, L.I., 2001c. Feeding and dissipative waves in fracture and phase transition. III. Triangular-cell lattice. J. Mech. Phys. Solids 49, 2839–2875.

Slepyan, L.I., 2005. Crack in a material-bond lattice. J. Mech. Phys. Solids 53, 1295–1313.

Symons, D.D., Fleck, N.A., 2008. The imperfection sensitivity of isotropic two-dimensional elastic lattices. J. Appl. Mech. – Trans. ASME, 051011-1-051011-8.

Torquato, S., Gibiansky, L.V., Silva, M.J., Gibson, L.J., 1998. Effective mechanical and transport properties of cellular solids. Int. J. Mech. Sci. 40, 71–82.

Wadley, H.N.G., 2006. Multifunctional periodic cellular metals. Philos. Trans. R. Soc. A – Math. Phys. Eng. Sci. 364, 31–68.

Zhang, Y.H., Xue, Z.Y., Qiu, X.M., Fang, D.N., 2008. Plastic yield and collapse mechanism of planar lattice structures. J. Mech. Mater. Struct. 3, 1257–1277.